Off-resonant absorption in bound-to-continuum *p*-type GaAs/$Al_xGa_{1-x}As$ quantum wells: Overcoming absorption saturation with doping

F. Szmulowicz,[1] T. Oogarah,[2] J. Ehret,[1] K. Mahalingam,[1] H. C. Liu,[2] S.M. Hegde,[1] J. Solomon,[1] D. Tomich,[1] G. Landis,[1] and G. J. Brown[1]

[1]*Air Force Research Laboratory, Materials and Manufacturing Directorate, Wright-Patterson Air Force Base, Ohio 45433-7707, USA*

[2]*Institute for Microstructural Sciences, National Research Council, Ottawa, Ontario K1A 0R6, Canada*

(Received 24 February 2003; published 8 August 2003)

Optimum bound-to-continuum normal-incidence absorption in low-doped (less than 1×10^{12} cm^{-2}) *p*-type GaAs/AlGaAs quantum wells obtains for well widths for which the second light-hole (LH2) level is resonant with the top of the valence band quantum well near the center of the Brillouin zone. Experimentally we found that such absorption saturates at higher doping levels. For higher doping around 4×10^{12} cm^{-2}, our envelope-function approximation (EFA) model predicts that pushing LH2 deeper into the continuum avoids absorption saturation and at least doubles the photoresponse. The results are explained on the basis of an EFA calculation, which shows that saturation is due to the fact that the line of resonances in the continuum as a function of the in-plane wave vector eventually becomes a bound LH2 band in the well at some critical wave vector. By matching this critical wave vector (via well width and/or well depth adjustment) with the Fermi wave vector (determined by doping in the well) for the desired QWIP (i.e., cutoff wavelength), saturation can be avoided. This prediction is verified on a set of well-characterized samples. A re-entrant band behavior, in which a band is bound over a limited portion of the Brillouin zone, is also demonstrated.

DOI: 10.1103/PhysRevB.68.085305 PACS number(s): 78.67.De, 73.21.Fg, 78.66.Fd, 85.60.Gz

I. INTRODUCTION

Absorption is a property governing the performance of opto-electronic devices such as radiation detectors. In the design of *p*-type GaAs/AlGaAs quantum-well infrared photodetectors (*p*-QWIPs), we have sought to optimize absorption as a function of the design parameters.[1–8] Unlike GaAs/AlGaAs *n*-QWIPs, *p*-QWIPs absorb normally incident light[9–14] without gratings, which simplifies processing of the material into focal planes. Thus, pixel size is not constrained by grating design. *p*-QWIPs can reach both 8–12 μm and 3–5 μm bands and even shorter wavelengths.[15] In the case of the GaAs/AlGaAs system, mid-IR wavelengths can be reached with the use of nonstrained QWs.[6] An added design flexibility is the possibility of combining long-wavelength infrared (LWIR) *n*-QWIPs and mid-wavelength infrared (MWIR) *p*-QWIPs on the same wafer for multispectral detection.[16] Other attributes of GaAs/AlGaAs *p*-QWIPS are their very low noise and lower dark currents (bound-to-continuum), especially when not in the thermally limited regime (no DX-defects in barriers, lower tunneling probability of heavy holes).[8] Because of the heavy hole mass, the Fermi energy increases slower with doping in *p*-QWIPs than in *n*-QWIPs, which makes possible greater doping in *p*-QWIPs, so that absorption can be enhanced without as rapid increase in dark current.[1–4]

In a series of papers,[1–8] we developed criteria for the design of optimal *p*-type (i.e., extrinsic) GaAs/AlGaAs quantum well infrared photoconductive detectors. Our best GaAs/AlGaAs MWIR *p*-QWIP has the 4.8 μm peak responsivity of 10 mA/W and a gain of $g=0.05$ at 30 V, the detectivity of $D^*_{peak}=3.5\times10^{11}$ cm $Hz^{1/2}$/W at 80 K, $T_{BLIP}=100$ K at 10 V, and a quantum efficiency of 5% in single pass.[6–8] With the use of resonant cavities,[17] the quantum efficiencies were quintupled to 25%.

In *p*-QWIPs, optimal absorption obtains when the second light-hole (LH2) level is coincident with the top of the well, a criterion that is also conducive to good subsequent transport of the photoexcited hole.[1–8] These rules were guided by the envelope-function approximation (EFA) calculations of these structures.[3] In the hope of raising absorption through increased doping in the well, we discovered in one study that quadrupling the doping merely doubled absorption.[7] This disappointing fact serves as the impetus for the present study in which we explain the sublinear dependence on doping and propose and demonstrate a sample design that provides for a linear increase of absorption with doping. We show that the sublinear doping dependence is found in samples where the LH2 state, while a resonance in the continuum at the center of the Brillouin zone, is a bound state in the well beyond a certain in-plane wave vector. The proposed *p*-QWIP design avoids absorption saturation by ensuring that the light-hole resonance is entirely in the continuum.

The rationale for the present investigation can be captured through the following simplified model of a *p*-type QWIP with decoupled, parabolic heavy-(HH) and light-hole (LH) bands. To avoid confusion with signs, the energy axis for holes is up and the zero of energy is at the well bottom. Consider a heavy hole with energy E, propagating in the barrier region. Its energy can be divided into motions in the growth direction ($\perp$) and in the plane of the QW ($\parallel$),

$$E=\frac{\hbar^2k_\parallel^2}{2m_\parallel^{HH}}+\frac{\hbar^2k_\perp^2}{2m_\perp^{HH}}+V_0, \tag{1}$$

where V_0 is the height of the barrier (i.e., the GaAs/AlGaAs valence band offset). The demarcation line between the free and the bound hole regions is defined by the condition,

$$k_\perp=0, \tag{2}$$

or, equivalently, by the energy

$$E_{\text{free}}^{\text{HH}} = \frac{\hbar^2 k_{\|}^2}{2m_{\|}^{\text{HH}}} + V_0 . \tag{3}$$

Further, let the band dispersion for the LH2 state be given by

$$E_{\text{LH2}}^0(k_{\|}) = \frac{\hbar^2 k_{\|}^2}{2m_{\|}^{\text{LH}}} + E_{\text{LH2}}^0, \tag{4}$$

where E_{LH2}^0 is the energy of the LH2 state at the center of the Brillouin zone—either a bound state, $E_{\text{LH2}}^0 < V_0$ (for which the band represent a line of bound states) or a resonance in the continuum, $E_{\text{LH2}}^0 > V_0$ (in which case the band is a line of resonances). The optimally designed *p*-QWIP was shown earlier[1–4] to have $E_{\text{LH2}}^0 \approx V_0$, for which the hole absorption and subsequent hole transport are both optimized. However, for the GaAs/AlGaAs QW, light-holes are heavier than the heavy holes in the in-plane direction,[18]

$$m_{\|}^{\text{LH}} > m_{\|}^{\text{HH}} . \tag{5}$$

As a result, even if $E_{\text{LH2}}^0 > V_0$, the LH2 line of resonances must at some $k_{\|} \equiv \kappa$ cross the top of the well and become a bound band i.e.,

$$\frac{\hbar^2 \kappa^2}{2m_{\|}^{\text{LH}}} + E_{\text{LH2}} \leqslant \frac{\hbar^2 \kappa^2}{2m_{\|}^{\text{HH}}} + V_0 . \tag{6}$$

In a coupled EFA model, such as the 8×8 EFA model to be presented later, the positions of LH bound bands are influenced not only by the different effective masses of the heavy and light holes but also by the band mixing.

Since optical transitions from the HH1 ground state are $k_{\|}$-conserving, it is important that the point of intersection κ be comparable with the Fermi wave vector, k_F. For $k_{\|} \geqslant \kappa$, the LH2 band becomes bound in the well and does not contribute to the bound-to-continuum absorption. In fact, the band pulls down most of the available oscillator strength with it as it enters the well as a bound state.

Another way of looking at this problem is to observe that the continua for the light and heavy holes [see Eq. (3)] are different,

$$E_{\text{free}}^{\text{HH}} = \frac{\hbar^2 k_{\|}^2}{2m_{\|}^{\text{HH}}} + V_0 \neq E_{\text{free}}^{\text{LH}} = \frac{\hbar^2 k_{\|}^2}{2m_{\|}^{\text{LH}}} + V_0 , \tag{7}$$

and, in fact, there is a region between the LH and HH continua where HH holes can propagate freely while LH holes can only be evanescent.[19–22] The width of this region increases with the in-plane wave vector. A HH hole incident on the well in this energy region can become bound in the well with an appreciable LH character.[19,20] Consequently, this is the region that is rich with resonant structures—bands of energies with enhanced probabilities of finding a hole in the well region.[19–22] Optical transitions to these bands of energies give rise to enhanced absorption. Whenever these resonant bands become bound states in the well, the bound-to-continuum absorption suffers, resulting in absorption saturation described in this paper.

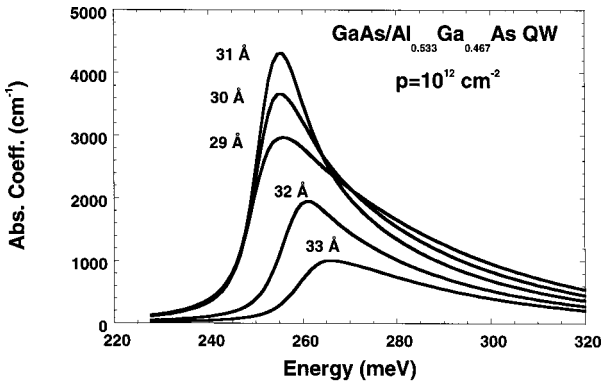

FIG. 1. Calculated absorption (on absolute scale) for the 3–5 micron GaAs/AlGaAs *p*-QWIP with the hole density of 1×10^{12} cm^{-2} ($k_F = 0.014$/Bohr) as a function of well width and photon energy at $T = 0$ K. The spectrum is shifted for exchange energy.

The main message of this paper is that one can avoid such a deleterious condition by pushing the LH2 resonance deeper into the continuum (i.e., away from the top of the well) depending on the degree of doping (i.e., the Fermi wave vector) and, to a lesser degree, on the operating temperature of the detector (which broadens the Fermi–Dirac distribution). The complete theory of this effect will be developed in this paper and the effect demonstrated on a set of specially designed samples.

In the rest of the paper, the energy axis for holes points downward. This paper is organized as follows: Section II provides the theoretical motivation for the research and the design of samples for testing the theory. Section III describes the growth of the samples and their characterization. The device measurements and comparison to theory are discussed in Sec. IV. Conclusions are presented last.

II. THEORY

Our previous work on MWIR *p*-QWIPs based on GaAs/AlGaAs MQWs was motivated by the optimization study[6] summarized in Fig. 1. Using our 8×8 EFA theory,[3] a number of absorption curves were calculated for different width *p*-QWIPs with the hole density of 1×10^{12} cm^{-2}. Here, the choice of a 31 Å MQW was found to be optimal for the 3–5 micron *p*-QWIP, for which the LH2 level is coincident with the top of the well at the center of the Brillouin zone. Our optimization studies are often calculated at 0 K since some of our photoresponse measurements are made near the liquid helium temperature and the calculated results are easier to interpret there. However, our device measurements are carried out near the liquid nitrogen temperature; for that reason, $T = 80$ K calculations will also be presented.

Guided by this design, a number of structures with different doping concentrations were grown to increase the absorption and to find the doping level for the highest BLIP operating temperature.[7] However, the experimental results indicated that quadrupling the carrier concentration from 1×10^{12} cm^{-2} to 4×10^{12} cm^{-2} only doubles the absorption.[7] This undesirable situation was explained by our calculation,

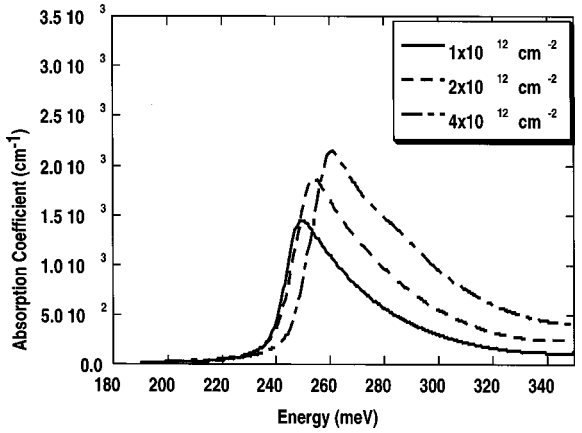

FIG. 2. The calculated $T=0$ absorption for three samples ($x=0.537$, 31.7 Å, corresponding to the parameters of the grown samples) grown to test the concentration dependence of *p*-QWIP response (Ref. 7). Here, quadrupling the doping (doubling the Fermi wave vector) only doubles the absorption. The spectrum is shifted for exchange energy.

Fig. 2, where the sample parameters are those of the actually grown samples, for which the well width was slightly wider and the well depth slightly deeper than in the proposed design. These small differences in the grown sample pulled the LH2 level slightly into the well making LH2 a bound state and thus unavailable for the bound-to-continuum absorption, which resulted in a sublinear dependence of photoresponse on doping. Our model, Fig. 2, was able to reproduce this behavior. In later work, we were able to quintuple absorption through the use of resonant cavities,[17] but the original goal of increasing absorption with doping was not met.

On closer examination, the design that served as the optimized design does shows quadrupled absorption at least up to $k_F=0.014$/Bohr ($p=1\times10^{12}$ cm^{-2}), Fig. 3. However, above that concentration, absorption saturates again. Thus, for $k_F=0.026$/Bohr ($p=4\times10^{12}$ cm^{-2}), there is no quadrupling from $k_F=0.014$/Bohr. As we showed earlier, *p*-QWIP detectivities and BLIP operating temperatures are optimized in this range of dopant concentrations.[7,8]

The saturation phenomenon seen in Fig. 3 can be best

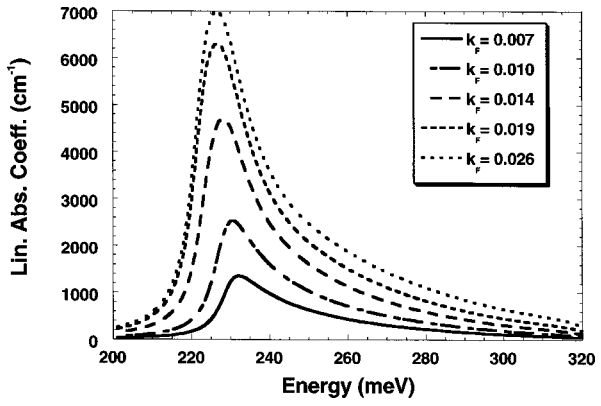

FIG. 3. The calculated $T=0$ K absorption for a center-zone optimized MWIR *p*-QWIP ($x=0.533$,$w=31$ Å) as a function of doping (2.5×10^{11} to 4×10^{12} cm^{-2}).

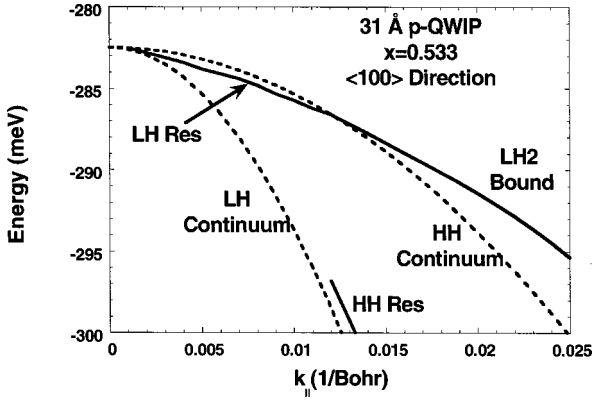

FIG. 4. The band structure for a 31 Å, $x=0.533$, *p*-QWIP (corresponding to sample G2-2735 in the text) near the top of the valence band, showing the LH2 bound band and lines of LH and HH resonance.

explained with reference to the band plot for the 31 Å *p*-QWIP, Fig. 4, for energies close to the top of the valence quantum well. First, as explained in the Introduction, the continuum for the light and heavy holes as a function of the in-plane wave vector begin at energies for which

$$\mathrm{Im}\, k_\perp(\mathbf{k}_\parallel, E)=0, \tag{8}$$

i.e., for nonevanescent states. Equation (8) generalizes the condition of Eq. (2) for the coupled band case in which complex propagation wave vectors are possible.[19–24] These energies are shown as dashed lines in Fig. 4. The position of the LH2 band and the continuum condition, Eq. (8), were calculated with the 8×8 EFA model. Clearly, the continuum for the lighter LH holes begins at higher hole energies than for the heavy HH holes, which was explained earlier in the Introduction on the basis of a simple uncoupled-band model.

Second, in the energy region between the dashed lines in Fig. 4, heavy holes are free to propagate in the barrier regions whereas light holes are evanescent. It is therefore possible for a heavy hole incident on the well from the barrier region to become quasibound in the well.[19–22] In our calculation, the continuum states are constructed from even and odd combinations of left- and right-incident hole states, i.e., the standard even- and odd-parity stationary states.[1–4] Whenever a hole becomes quasibound in the well, there is an enhanced probability of finding the hole in the well region, i.e., there is a resonance. Therefore, the resonance condition can be traced by examining the wave function of the hole as a function of energy and parallel wave vector.[3] Alternately, in the scattering language, one can examine the hole reflectivity/transmittivity for the given scattering channel (heavy-, light-, or spin–orbit-holelike). In our stationary state representation, reflectivities can be obtained from proper sums or differences of the even and odd stationary states. Photoexcitation of holes from lower subbands to these resonant states naturally leads to higher absorption probability.

Third, it must be said that the resonance condition is not easy to identify in the calculation. The resonances are most distinct—large and sharp (on the order of an meV)—away from the center of the Brillouin zone, where in effect the well

for light holes is deeper (i.e., the spread between the HH and LH continua is wider). These resonant peaks sit atop a background of nonresonant states.[12,19–22] Closer to the zone center, these regions of enhanced probability of finding a hole in the well region broaden considerably and are subsumed within the nonresonant background. In the present paper, we follow the maxima of the hole probability density in the well as close to the center of the Brillouin zone as possible; however, at times, these maxima become indistinct.

Fourth, a word of caution is in order regarding the relation of resonances to bound states in the present coupled-band formalism. Bound states descend from the continuum into the well as the well is made wider or deeper. In a simple one-band model, the density of states in the continuum is normally zero at the top of the well unless a bound state is about to descend out of the continuum into the well.[25] In the present 8×8 EFA calculation, bound states detach themselves from the continuum of nonresonant states in a similar manner. Still, it is very difficult to follow the emergence of a band out of the continuum at the center of the Brillouin zone, e.g., LH2 band, until it appears as a bound band.

Lastly, it is well-established that in some cases the 8×8 EFA model can produce spurious bands.[26] These bands are the result of the fact that the 8×8 model must return four doubly degenerate propagation vectors $k_\perp$, whereas only three are physically meaningful for holes.[24,26,27] The wave function in the EFA model is a superposition of exponentials of the form $\exp(ik_\perp z)$, thus the possibility of spurious solutions with unphysical exponents.[26,27] In GaAs/AlGaAs QWs, the extra propagation vectors are large and pure imaginary and decay very fast away from the well interfaces, causing no problem to the physics.[3] As an extra precaution, the calculation was repeated using a 6×6 model with no explicit coupling to the conduction band, thereby eliminating the extra propagation vectors in the problem. The 6×6 EFA calculation confirmed the existence of the resonances, albeit at energies shifted from those found in the 8×8 EFA model.

Figure 4 shows a line of LH-like resonances merging into a bound LH2 band as a function of the in-plane wave vector. The crossover point for the 31 Å p-QWIP takes place at 0.013/Bohr, which is on the order of the Fermi wave vector for the doping of $p=1\times10^{12}$ cm^{-2} ($k_F=0.014$/Bohr). Once the LH2 band becomes bound, it becomes unavailable as the final state in the bound-to-continuum absorption. Because of the *f*-sum rule, the LH2 band pulls down a considerable amount of oscillator strength (about half, according to our calculation) with it, further weakening the bound-to-continuum absorption. Beyond the crossover point, wave vector-conserving optical transitions from lower subbands proceed to states in the continuum that have lower oscillator strengths. As a result, absorption in Fig. 3 saturates as a function of doping (i.e., the Fermi wave vector). Appendix A contains a few more cases of resonances in GaAs/AlGaAs p-QWIPS, including an interesting reentrant band phenomenon.

Figure 4 suggests that absorption saturation can be circumvented by pushing the LH2 band into the continuum over larger regions of the Brillouin zone, which can be accomplished by narrowing the well. However, narrowing the well necessarily weakens the resonance condition near the center of the Brillouin zone. For example, Fig. 5 shows the band diagram for a 29 Å p-QWIP, for which the LH2 band is no longer bound and a LH-like resonance appears in the region between the LH and HH continua over the entire reciprocal space examined. The trade off is best examined by doing an actual calculation to find the optimum sample design for the given doping level. Here, the doping level corresponding to $k_F=0.026$/Bohr ($p=4\times10^{12}$ cm^{-2}) is of interest. Figure 6 shows the calculated absorption for the doping level of $p=4\times10^{12}$ cm^{-2}, with other parameters kept constant. Here, the 29 Å design, for which the LH2 level is slightly above the well top, is found to be optimum, although the peak absorption is slightly redshifted. For a 100-well MQW, Fig. 6 predicts a 30% single pass quantum efficiency. At the same time, the 31 Å, design, which was optimum at $p=1\times10^{12}$ cm^{-2}, is found to be inferior. While the 29 Å design is better at $p=4\times10^{12}$ cm^{-2}, Fig. 6, and worse at $p=1\times10^{12}$ cm^{-2}, Fig. 1, than the 31 Å design, at $p=2\times10^{12}$ cm^{-2}, the two are equivalent. Moreover, absorption for the 29 Å sample does not saturate below $p=4\times10^{12}$ cm^{-2}. The doping of $p=2\times10^{12}$ cm^{-2} was found earlier to optimize the detectivity and the BLIP temperature of MWIR p-QWIPs.[7,8] For practical concerns, absorption in Fig. 6 is seen to be less sensitive to width variations on the narrower side of the optimum design.

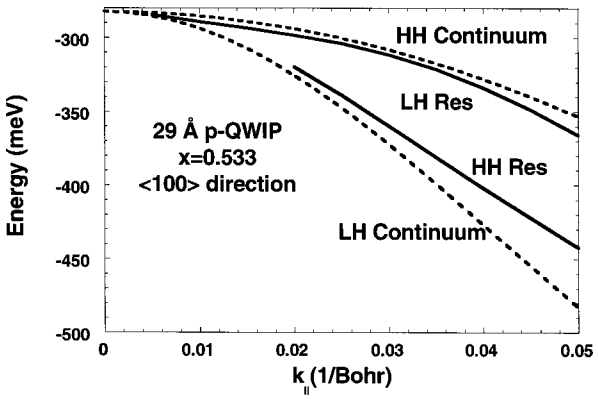

FIG. 5. The band structure for a 29 Å, $x=0.533$, p-QWIP near the top of the valence band, showing the lines of LH and HH resonances; LH2 is no longer a bound state.

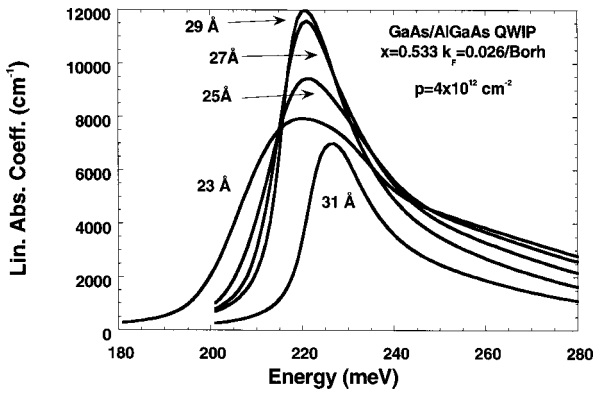

FIG. 6. Absorption of p-QWIPs with $x=0.533$ as a function of well width for $p=4\times10^{12}$ cm^{-2} ($k_F=0.026$/Bohr) at $T=0$ K.

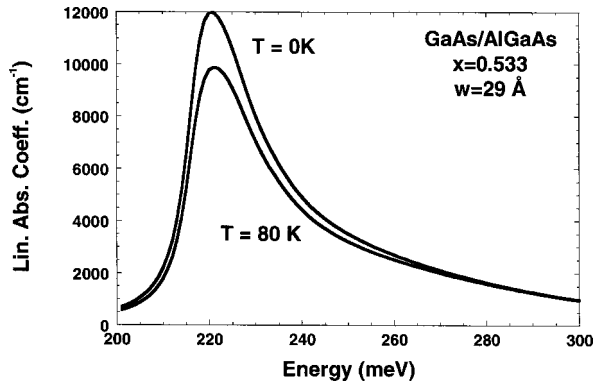

FIG. 7. The calculated temperature dependence of absorption for the 29 Å GaAs/AlGaAs, $x=0.533$, p-QWIP.

Another important issue is the temperature stability of a device. Figure 7 shows the calculated absorption for the 29-Å designs. The 29 Å MQW suffers only a 20% decrease in absorption from 0 K to LN_2, while the 31 Å design with $p=1\times10^{12}$ cm^{-2} suffers a 40% decline,[20] making the new design all the more desirable. The reason for the large temperature variability is again connected with the band diagram, Fig. 4: a temperature increase promotes holes to higher energies (thus larger in-plane momenta) along the HH1 ground state subband; photon excitations from these states proceed to states in the continuum that are nonresonant in nature since the LH2 band is bound at larger wave vectors.

Since the device measurements in Sec. IV include data on the polarization dependence of photoresponse, the polarization dependence of the calculated absorption is discussed next. The polarization dependence of absorption for the 31 and 29 Å p-QWIPs with $p=4\times10^{12}$ cm^{-2} at 80 K is shown in Figs. 8 and 9, respectively. Clearly, the S/P ratio changes depending on the resonance condition, i.e., whether LH2 is bound in the well or is a continuum resonance. The S/P ratio changes from about 5/3 for the 31 Å QWIP to about 10/9 for the 29 Å QWIP. Continuing the trend, for a 27 Å p-QWIP, the S/P ratio is 5/6, i.e., less than one. A previously unoptimized sample, G2-2492, had the S/P ratio of 5/3, both as calculated and verified by experiment,[6] which is consistent with Fig. 8.

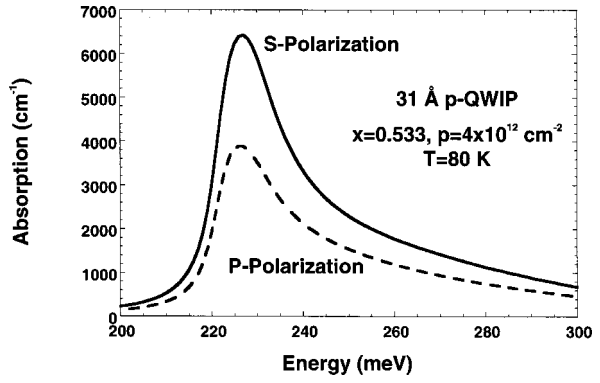

FIG. 8. The calculated optical absorption for the 31 Å ($x=0.533$) QWIP (corresponding to sample G2-2735 in the text. for different polarizations defined with respect to the 45° facet.

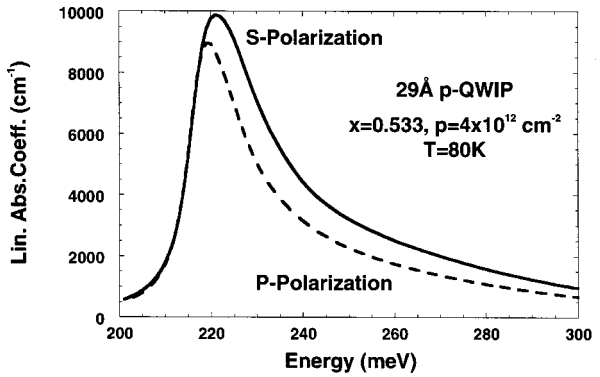

FIG. 9. The calculated optical absorption of the 29 Å ($x=0.533$) QWIP for different polarizations defined with respect to the 45° facet.

Figures 8 and 9 demonstrate that, whenever optical transitions originate from extended regions of the Brillouin zone away from the zone center, the polarization selection rules[11] are weakened because of the greater hybridization of the heavy and light hole bands away from the zone center, which makes the S and P spectra comparable. For the ''zone center-optimized'' samples, the S spectrum dominates the P-spectrum.

Figure 6 suggests a scheme for enhancing the performance of p-QWIPs and at the same time verifying the predictions of the theory. Based on Fig. 6, growing samples with 27 and 31 Å wells ($x=0.533$,$p=4\times10^{12}$ cm^{-2}), on either side of the best design at 29 Å, should dramatically demonstrate the tradeoff between the strictly resonant design around 31 Å and the slightly off-resonant 29 Å MQW. Sample growth and device measurements are discussed next.

III. SAMPLE GROWTH AND CHARACTERIZATION

A. Sample growth

Two new samples designated as G2-2735 (31 Å QW) and G2-2736 (27 Å QW) were grown by MBE to theoretical specifications with the hope of eliminating absorption saturation and at least doubling absorption. The growth detail is the same as before.[6–8] The layer sequence is listed in Table I. The MQW consists of 100 repeats of the layers specified in bold letters. Beryllium doping is expected to diffuse throughout the well, which is why doping is stopped 7 Å from the trailing edge of each QW. From *in situ* monitoring of growth parameters, we expect at worst a 1 Å difference in the well width and a 0.01 difference in the barrier Al fraction from the design values. The beryllium concentrations dialed in during molecular beam epitaxy (MBE) growth are based on standard calibration curves.

During the growth run for sample G2-2735, the well thickness decreased by 0.8%, the barrier thickness increased by 0.3%, and the aluminum mole fraction went from 0.522 to 0.527. During the growth of sample G2-2736, the well thickness increased by 1.2%, the barrier thickness did not change, and the aluminum mole fraction decreased from 0.525 to 0.519. All changes are estimated from the third decimal place in the growth rate measurements.

TABLE I. The layer sequence for samples G2-2735 and G2-2736. The layers in bold letters are repeated 100 times to form the MQW. The doping in inserted as a sheet, 7 Å away from the nearest QW wall, with the empirical expectation that beryllium will diffuse throughout the well.

	G2-2735		G2-2736	
	Thickness (Å)	x	Thickness (Å)	x
SI GaAs substrate		0		0
GaAs:Be (8×10^{18} cm^{-3})	6000	0	6000	0
GaAs	20	0	20	0
AlGaAs	**200**	**0.52**	**200**	**0.52**
GaAs	**7**	**0**	**7**	**0**
Delta doping	**4×10^{12} cm^{-2}**		**4×10^{12} cm^{-2}**	
GaAs	**24**	**0**	**20**	**0**
AlGaAs	200	0.52	200	0.52
GaAs:Be (8×10^{18} cm^{-3})	2000	0	2000	0

Based on the *in situ* monitoring before and after the growths, there is at worst a 1 Å difference from the design for the well width and 0.01 difference in barrier Al fraction. These two factors may be self-compensating considering their effect on the bound-to-bound vs bound-to-continuum absorption, i.e., in the worst case, we have

$$\text{for G2-2735:} \quad 31\ \text{Å} \rightarrow 30\ \text{Å} \quad x = 0.52 \rightarrow 0.53,$$

$$\text{for G2-2736:} \quad 27\ \text{Å} \rightarrow 28\ \text{Å} \quad x = 0.52 \rightarrow 0.51,$$

so that well narrowing is compensated by well deepening, which has opposite effects on the positions of the energy levels in the well.

Because of the sensitivity of the model predictions to the actual sample parameters, it is important to ascertain the physical parameters of the samples. In the next subsections, we summarize the results of x-ray diffraction, photoluminescence, TEM, and SIMS measurements.

B. X-ray diffraction

The theta-omega plots from x-ray measurements for Sample G2-2736 is provided in Fig. 10 (the plot for G2-2735 is similar). The large number of narrow superlattice satellite peaks attests to the high quality of the grown structures. Numerical simulations of the x-ray data for the two samples are given in Table II.

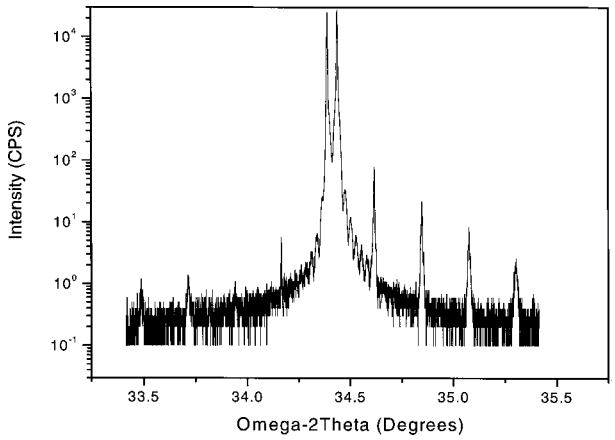

FIG. 10. X-ray data for sample G2-2736.

These x-ray data fitting simulations confirm that the target alloy concentration of 0.52 was achieved and the barrier widths were within 2% of the target design. However, the well width estimates were 35.5 Å and 35 Å for samples G2-2735 and 2736, respectively, which indicates no difference in the two growths. More sensitive techniques (see Sec. III C) clearly show that, in fact, the two p-QWIPs are different. We take this as an indication of the difficulty of fitting x-ray data on these particular p-QWIPs since the determinations of well widths and aluminum mole fractions are interdependent.

C. Photoluminescence investigation

Two p-QWIP samples, G2-2735 and G2-2736, were prepared for low temperature photoluminescence (PL) experiments by cutting them to size 3/8 in.$\times$3/8 in. The top contact layer ($\sim$6000 Å, Be-doped GaAs) was etched off, leaving a thin layer of GaAs:Be on top of the MQW detector structure. Both samples were mounted, strain free, in a continuous flow liquid helium cryostat. The samples were in a flowing helium

TABLE II. Simulation of x-ray data for samples G2-2735 and G2-2736. Layers in boldface letters are repeated 100 times.

	G2-2736		G2-2735	
	Thickness (Å)	x	Thickness (Å)	x
GaAs substrate	infinite	0	infinite	0
GaAs	6000	0	6000	0
AlGaAs	**200**	**0.52**	**200**	**0.52**
QW GaAs	**26.750**	**0**	**26.50**	**0**
GaAs	**8.75**	**0**	**8.5**	**0**
AlGaAs	214	0.52	213.5	0.52
GaAs	20	0	20	0
GaAs	2000	0	2000	0

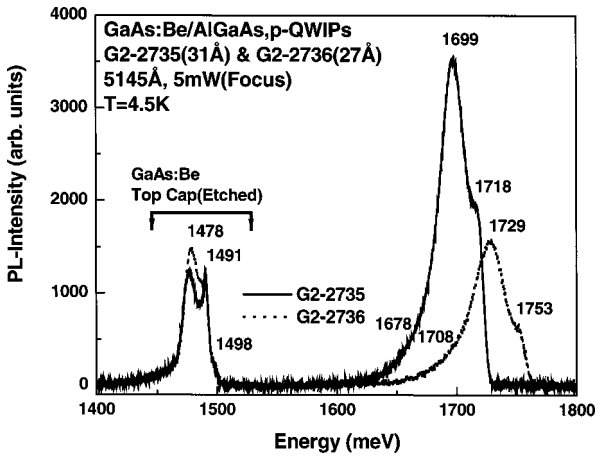

FIG. 11. Low temperature (4 K) PL-spectra for *p*-QWIPs G2-2735 and G2-2736.

vapor and were maintained at 4.5 K. A CW, argon-ion laser at 5145 Å was used as the above band gap excitation source. The average power from the laser was 5 mW and the beam was slightly defocused (beam diameter ~1.5 mm) on the sample. The PL signal in the near IR region was detected with a Si-avalanche detector and analyzed using a Bomem DA-3 Fourier transform spectrometer. The resolution of the instrument was set to 1 cm^{-1} and 64 scans were co-added to obtain the PL-spectra. The spectra for both samples are discussed individually below.

1. Sample G2-2735

The PL signal from the *p*-QWIP sample G2-2735 is shown in Fig. 11. The spectrum in the region 1450–1510 meV is from the Be-doped GaAs top contact layer. The strong MQW-related signal is in the 1600–1775 meV region. A Gaussian fit analysis was carried out to locate the individual peak positions and their full width at half maximum (FWHM). The 36 meV-broad peak centered at 1678 meV corresponds to the free-to-beryllium acceptor bound transition. The dominant peak at 1699 meV with the FWHM of 21 meV is assigned to the C1-HH1 transition. Its position is within 5 meV of a model 8×8 EFA calculation for the C1-HH1 transition corrected for a 2D screened exchange[28] due to the large *p*-doping in the wells, Table III.

The weaker peak at 1718 meV, with the FWHM of 9 meV, on the high-energy shoulder of C1-HH1 is similar to the feature described by Monemar's[29–31] group in heavily *p*-doped MQWs. This feature, however, is not related to the C1-LH1 transition, since LH1 in our narrower samples is quite far separated from the Fermi edge (see Table III). The samples investigated by Monemar were much wider, with the LH1 level intersecting the Fermi edge. Their interpretation, therefore, does not fit our case.

2. Sample G2-2736

The PL signal from the *p*-QWIP sample G2-2736 is also shown in Fig. 11. The spectrum in the region 1450–1510 meV is from the Be-doped GaAs top contact layer as before. The strong, MQW signal is in the 1600–1775 meV region. The broad peak centered at 1708 meV with the FWHM at 46 meV is again attributed to the free-to-beryllium acceptor bound transition. The dominant peak at 1729 meV with the FWHM of 25 meV is assigned to the C1-HH1 transition. As in G2-2735, the weaker peak at 1753 meV on the high-energy shoulder of C1-HH1 is similar to the feature described by Monemar's group[29–31] but is clearly unrelated to the C1-LH1 exciton.

3. Modeling the PL data

In order to model the PL peak positions, the energy levels of both electrons in the conduction band and holes in the valence band of the *p*-QWIPs were calculated using our 8×8 EFA model.[3] Then, we included a screened exchange energy for the hole gas based on the nominal beryllium doping density in the well and the bound exciton binding energy of 7 meV.[28] The results are summarized in Table III. The agreement between experiment and theory in Table III indicates that the nominal sample parameters are close to the design parameters, giving us added confidence in the parameters of the grown samples. Since the 7-meV exciton binding energy is an upper bound appropriate to the unscreened exciton, using a smaller number would improve the theoretical-experimental agreement in the table. The agreement between the PL peak positions and the model results is the strongest confirmation of the nominal growth parameters in Table I.

In addition, from the calculated values of the LH1 positions, we conclude that the sharp peak on the high-energy

TABLE III. Calculated energy levels and PL peak positions for samples G2-2735 and G2-2736.

	Sample G2-2735	Sample G2-2736
Ave. Al content in growth	0.525	0.522
Average well width	31	27
HH1	−51.91 meV	−62.02 meV
LH1	−108.33 meV	−122.69 meV
C1	1671.71 meV	1602.07 meV
Screened 2D exchange	17.94 meV	21.46 meV
Theor. PL peak	1697.7 meV	1724.63 meV
Expt. PL peak	1699 meV	1729 meV
Chem. Pot. 0 K (80 K)	−83.30 (−81.05) meV	−88.40 (−86.22) meV

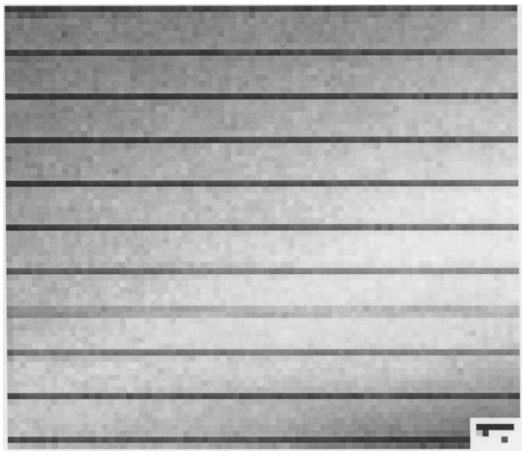

FIG. 12. TEM image of sample G2-2736; 10 periods.

side of the main PL peak cannot be ascribed to the C1-LH1 free exciton, as the LH1 level is separated by some 60 meV from the HH1 level as compared to the 10 meV separation of the PL peaks.

D. TEM results

Two TEM images of sample G2-2736 are shown in Figs. 12 and 13. The first image is a low-resolution (dark-field) image showing the GaAs (dark) and AlGaAs (bright) layers (the image shows 10 periods). The AlGaAs layer-thickness measured from this and other images is around 20.2 nm ± 0.6 nm.

The second image, Fig. 13, is a high-resolution TEM image showing a GaAs QW. The average layer thickness from several such images was around 2.87 nm$\pm$0.3 nm. Some regions show a 1–1.5 monolayer fluctuation in the layer thickness in the doped region.

However, the TEM profiles for sample G2-2735 were much rougher than for sample G2-2736. To within one monolayer, the thickness of quantum wells for this sample was about 12 monolayers, which is $12\times2.85=34.2$ Å ± 3.0 Å. This is outside the design specification of 31 Å, which is still within the error bar of the TEM measurements. The barrier widths were measured to be 208 Å$\pm$5 Å.

Overall, the TEM results for this sample indicate that the growth parameters are close to the design parameters, especially for sample G2-2736. The quality of the interfaces is sufficient to test the predictions of the theory.

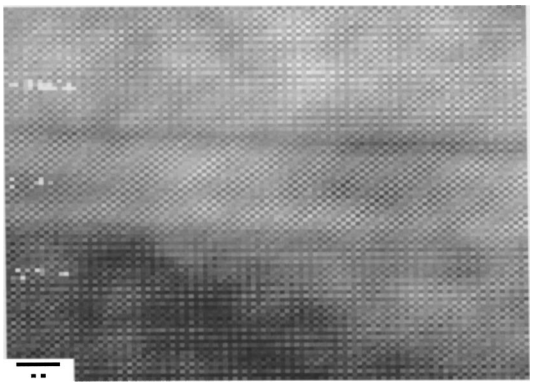

FIG. 13. TEM image of one period of sample G2-2736.

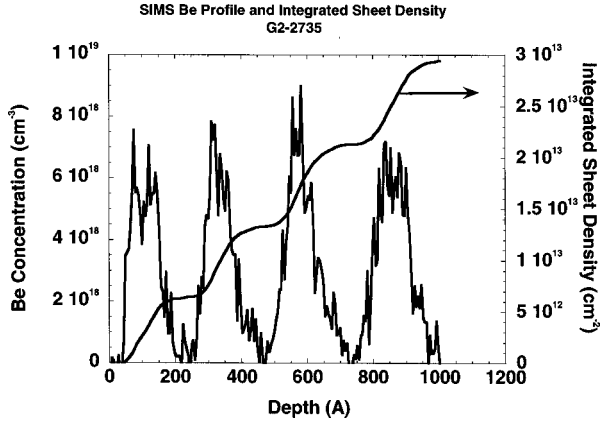

FIG. 14. Beryllium SIMS profile of sample G2-2735 and integrated profile. The profile for G2-2736 is similar.

E. SIMS measurements

SIMS measurements for the Be doping densities are shown in Fig. 14 for sample G2-2735 (data for G2-2736 are similar). The numerical values for Be concentrations are based on a previous round-robin calibration study, while the depth axis is based on the a *priori* knowledge of the expected $\sim$230 Å periodicity of the MQW.

Clearly, SIMS cannot resolve the sharp doping profiles inside the 3 nm QWs, but shows the 20 nm repeat period of the MQW quite well. The profile quality for sample G2-2735 indicates a rougher starting surface, thus a lower quality growth for that sample. This appears to be confirmed by the rougher interface quality in the TEM profiles for this sample (Fig. 14). However, our PL results appear insensitive to this interface quality. Integrating the depth profiles, the upper bound (because of the shape of the SIMS crater) on Be concentrations was established to be around 7×10^{12} cm^{-2}. As importantly, the sheet concentrations derived from the SIMS measurement on G2-2735 and 2736 were within 10% of each other.

Overall, the experimental results indicate that the two samples were grown very close to the theoretical specifications, although there is some disagreement between the PL and TEM results.

IV. DEVICE MEASUREMENTS

Device measurements were performed on samples in the shape of mesas with a top ring and a bottom contact.[6–8] We used polished facets to allow back-side illumination geometry with an internal angle of incidence of 45° and thus were able to measure the photocurrent as a function of incident light polarization. The photocurrent spectra were taken on a Fourier transform interferometer with a KBr beamsplitter and a globar source. The responsivity calibration was done with a 1000-K blackbody source and a variable narrow bandpass filter. The spectral response measurements for samples G2-2735 and G2-2736 as a function of wave number at 77 K

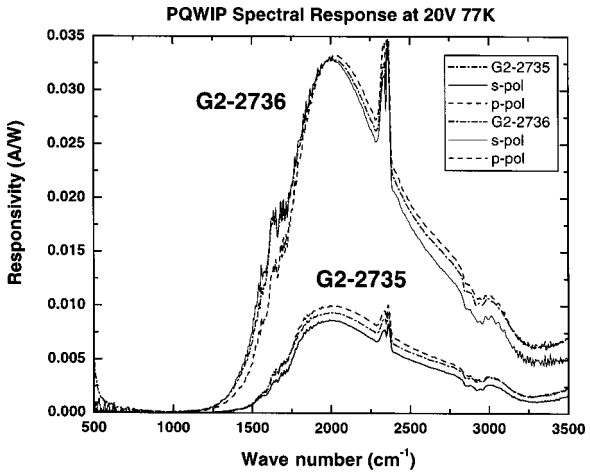

FIG. 15. Spectral photoresponse of samples G2-2735 and G2-2736 measured at 77 K at the bias voltage of 20 V. Both S-polarized (solid curve) and P-polarized (dashed curve) and unpolarized (dashed–dotted) spectra are shown. The peaks at about 2350 cm^{-1} are due to CO_2 absorption in the optical path. The spectra were collected by taking ratios into a reference spectrum.

are shown in Fig. 15. The spectrum for the 27 Å QWIP is narrower and about three times greater than that for the 31 Å sample.

The calculated absorption in Fig. 6 predicts at most a doubling of the spectral photoresponse. The additional improvement over the expected doubling for the 27 Å QWIP might be due to the better quality of sample G2-2736 (i.e., the better quality of its interfaces observed in TEM micrographs and SIMS results) and thus its better transport properties. Also, since the resonance in G2-2736 is higher above the barrier, the carrier sweepout in this sample is improved, hole capture and recapture are inhibited, which also leads to better gain, thus better photoresponse.

The tripling of the peak photoresponse at 77 K in going from G2-2735 to G2-2736, Fig. 15, continues as a function of voltage, Fig. 16. The symmetrical $I-V$ characteristics for

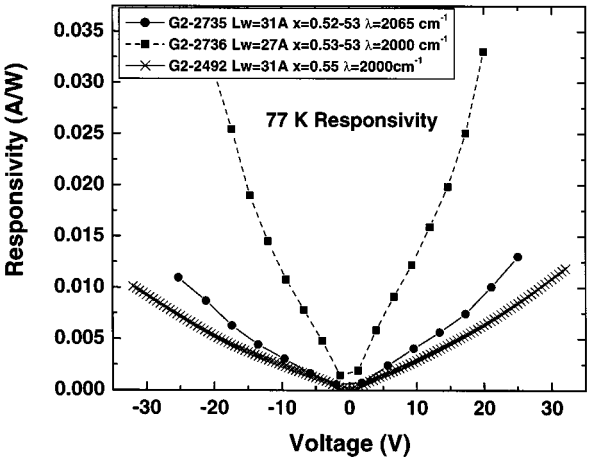

FIG. 16. Responsivity vs voltage at the peak spectral response at 77 K for G2-2735, G2-2736, and an earlier measured sample G2-2492 (sample C of Ref. 7).

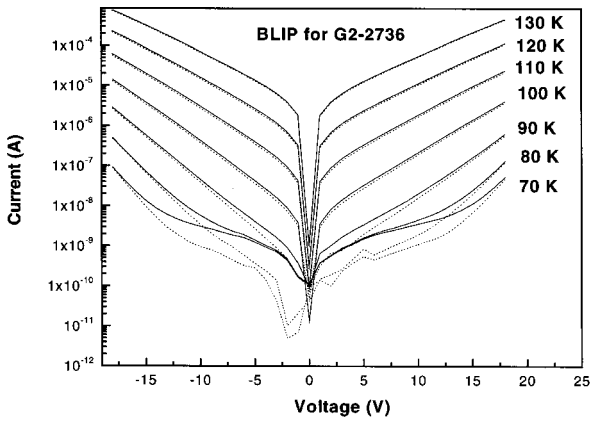

FIG. 17. Background (solid curves) and dark (dashed curves) current vs voltage as a function of temperature at the peak spectral response for sample G2-2736.

both samples in Fig. 20 indicates that both MQWs have symmetrical interfaces, further attesting to the good quality of their growth. Altogether, Figs. 15 and 16 support the model prediction that the new slightly off-resonant design is superior to the strictly resonant design.

Another piece of information is provided by the polarization dependence of photoresponse. The calculated polarization dependence for samples G2-2736 and G2-2735 was shown in Figs. 8 and 9. By comparison, our earlier polarization study of a lesser-doped sample—sample NRC-2 with 31 Å, $x=0.533$, $p=1\times10^{12}$ cm^{-2}, which was optimized at zone center—gave the S/P ratio of 5/3 both experimentally and theoretically.[6] For the slightly off-resonant sample G2-2736 (27 Å QWIP), the theoretical S/P ratio is nearly 5/6, which to within experimental accuracy is nearly 1. For G2-2735 (31 Å QWIP), the calculated S/P ratio is 5/3. Therefore, the S/P ratio is a sensitive test of the position of the LH2 resonance.

The polarization dependence of the measured photoresponse for samples G2-2735 and G2-2736, Fig. 15, is less pronounced than indicated by theory. This absence of strong polarization dependence in the measured spectra, especially

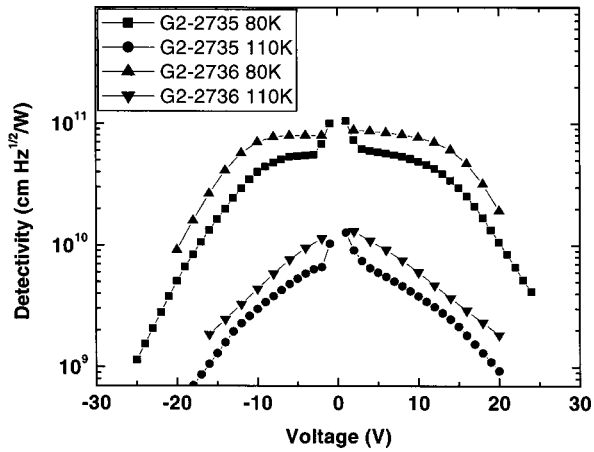

FIG. 18. The detectivity of samples G2-2735 and G2-2736 vs voltage at 80 and 110 K.

for sample G2-2735, cannot be reconciled with the earlier measured S/P ratio of 5/3 for sample NRC-2. We suspect that light depolarization from scattering by mesa edges could have been the cause of the polarization insensitivity of the measured photoresponse. For sample G2-2735, we also invoke its greater interface roughness (as supported by the poorer quality of its TEM and SIMS micrographs) to explain the greater disagreement between experiment and theory for this sample. Therefore, this part of the study is incomplete.

The operating temperature for G2-2736 was determined on the basis of the $I-V$ characteristics, Fig. 17, in the dark (dashed curves) and in the presence of background radiation (continuous curves) as a function of temperature. At 100 K, the two curves are indistinguishable, indicating that the thermally generated current is equal to the background photon generated current. Therefore, the operating temperature of the detector is below 100 K but above 90 K. Earlier, we studied a MWIR *p*-QWIP with the doping of 2×10^{12} cm^{-2}, for which the operating temperature was determined to be 100 K at 10 V.[7,8] So, the new design suffers a small decrease in the operating temperature, but this was to be expected since its greater doping necessarily raised its Fermi level, with the concomitant increase in the thermally generated current.

Lastly, we show Fig. 18, which compares the detectivities of samples G2-2735 and G2-2736. The peak detectivities of both samples are about $D^*_{\text{peak}}=1\times10^{11}$ cm Hz$^{1/2}$/W at 80 K; at 110 K, the detectivities drop down one order of magnitude. Our best MWIR *p*-QWIP with $p=2\times10^{12}$ cm^{-2} had $D^*_{\text{peak}}=3.5\times10^{11}$ cm Hz$^{1/2}$/W at 80 K,[7,8] which, because of its lesser doping, is greater than for G2-2736.

V. CONCLUSIONS

This study was motivated by the observation that MWIR *p*-QWIPs can suffer absorption saturation with doping. Based on an 8×8 EFA calculation, a new optimization scheme was proposed for GaAs/AlGaAs *p*-QWIPs, one that does not suffer from absorption saturation. Our calculation shows that there is a certain critical well width below which the LH2 band is a bound state in the well over the entire Brillouin zone. For slightly narrower widths, the LH2 is a resonance near the center of the Brillouin zone and a bound band beyond a certain critical wave vector. This situation holds for the QWIPs that suffer from absorption saturation with doping (e.g., sample NRC-2 and G2-2735). When doping is such that the Fermi wave vector is larger than this critical wave vector, absorption saturation ensues, since the final states in the continuum are nonresonant. For yet narrower wells, the light-hole derived states are resonances in the continuum over the relevant regions of the Brillouin zone (i.e., at least up to the Fermi wave vector). By making the light-hole-related states slightly off-resonant in the continuum, at least a twofold increase in absorption can be realized. It is predicted that single pass absorption of 30% can be realized for a 100-well MQW at 80 K with the slightly off-resonant design.

We tested this model prediction by growing two samples by MBE and thoroughly characterizing them. The sample corresponding to the new design had a three times stronger photoresponse than the sample corresponding to the strictly resonant design. Unlike the calculated results, the measured spectra were found not to be polarization sensitive, which we ascribe to depolarizing scattering of light from mesa edges. The calculation indicates that transitions near the center of the Brillouin zone are most polarization sensitive. The operating temperature for the slightly off-resonant design was found to be between 90 and 100 K, and the 80 K detectivity was about $D^*_{\text{peak}}=1\times10^{11}$ cm Hz$^{1/2}$/W, somewhat worse than for our previous best MWIR design with $p=2\times10^{12}$ cm^{-2}.

In other observations, QW bands need not emanate from the center of the Brillouin zone. In fact, cases were shown were bound bands start and stop away from the zone center. In addition, in our samples, the sharp peak on the high-energy side of the main C1-HH1 peak in PL cannot be ascribed to the C1-LH1 free exciton transition. This observation is relevant to further studies of Fermi-edge singularities in *p*-doped quantum wells.

ACKNOWLEDGMENTS

The work of F.S. and his University of Dayton Research Institute co-workers was supported by the Air Force Contract No. F33615-00-C-5422 at the Materials Laboratory. We would like to thank P. Chow-Chong, M. Byloos, and M. Buchanan for device microfabrication. The work at the NRC was supported in part by DND.

APPENDIX

This appendix makes a number of observations about the interplay of bound bands and resonances. Figure 4 shows a resonance in the continuum continuing as a LH2 bound band for a 31 Å GaAs well surrounded by AlGaAs barriers with aluminum concentration of $x=0.533$. It is common for quantum well calculations to follow bands from the origin of the Brillouin zone. Tracing the evolution of the band structure, Fig. 5 shows how for the narrower well width of 29 Å, the bound LH2 band is pushed out from the well and a resonance appears in the continuum. Conversely, going from the 29 Å

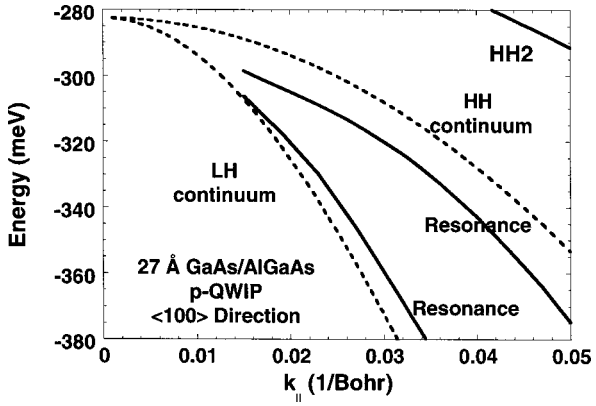

FIG. 19. The band structure for a 27 Å, $x=0.533$, *p*-QWIP (corresponding to sample G2-2736) near the top of the valence band. The LH2 band has been pushed out into the continuum.

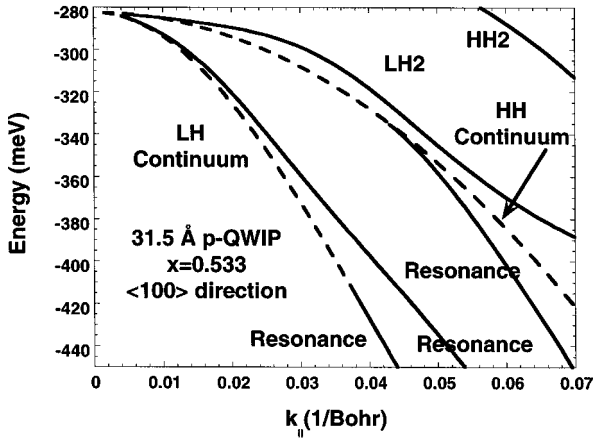

FIG. 20. The band structure for a 31.5 Å, $x=0.533$, *p*-QWIP near the top of the valence band. The LH2 band is bound over the entire Brillouin zone.

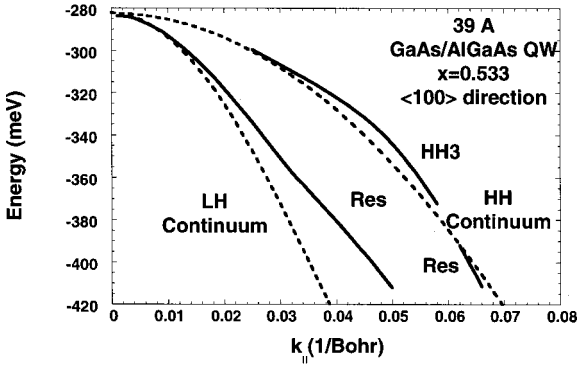

FIG. 21. The band structure for a 39 Å, $x=0.533$, *p*-QWIP near the top of the valence band. LH2 is totally bound while the HH3 band is bound over a limited portion of the Brillouin zone, not including the origin.

to 31 Å well, one can view the descent of LH2 into the well from the continuum as the consequence of a lower HH2 band (not shown in Fig. 4) moving deeper into the well. Since away from the zone center, HH and LH bands are of a mixed character, they necessarily repel. Once the HH band moves deeper, the LH band can move deeper as well. In Fig. 19, for a 27 Å well (corresponding to sample G2-2736 in the text), the resonances are pushed higher into the continuum as the HH2 band nears the top of the well. For a well slightly wider than 31 Å, Fig. 20, the LH2 band is bound over the entire Brillouin zone, and the continuum resonances have also descended in energy.

Lastly, in Fig. 21, a more complicated situation is shown for a 39 Å well, where a number of bound bands and resonances are seen. In particular, the HH3 band is bound over a limited portion of the Brillouin zone, not including the origin! This phenomenon of reentrant bands is interesting in its own right, and this phenomenon has not been reported heretofore. This richness of the QW band structure in the bound and continuum regions is owed to the coupled band behavior of GaAs/AlGaAs valence bands.

[1] G. J. Brown and F. Szmulowicz, in *Long Wavelength Infrared Detectors*, edited by Manijeh Razeghi (Gordon and Breach, Philadelphia, 1996).
[2] Gail J. Brown, F. Szmulowicz, and S. M. Hegde, J. Electron. Mater. **24**, 559 (1995).
[3] F. Szmulowicz and G. J. Brown, Phys. Rev. B **51**, 13 203 (1995).
[4] F. Szmulowicz and G. J. Brown, Appl. Phys. Lett. **66**, 1659 (1995).
[5] H. C. Liu, L. Li, M. Buchanan, Z. R. Wasilewski, G. J. Brown, F. Szmulowicz, and S. M. Hegde, J. Appl. Phys. **83**, 585 (1998).
[6] H. C. Liu, F. Szmulowicz, Z. R. Wasilewski, M. Buchanan, and G. J. Brown, J. Appl. Phys. **85**, 2972 (1999).
[7] A. Shen, H. C. Liu, F. Szmulowicz, M. Buchanan, M. Gao, G. J. Brown, and J. Ehret, J. Appl. Phys. **86**, 5232 (1999).
[8] A. Shen, H. C. Liu, M. Buchanan, M. Gao, F. Szmulowicz, G. J. Brown, and J. Ehret, J. Vac. Sci. Technol. A **18**, 601 (2000).
[9] B. F. Levine, S. F. Gunapala, J. M. Kuo, S. S. Pei, and S. Hui, Appl. Phys. Lett. **59**, 1864 (1991).
[10] P. Man and D. S. Pan, Appl. Phys. Lett. **72**, 1539 (1992).
[11] Y. C. Chang and R. B. James, Phys. Rev. B **39**, 12 672 (1989); F. Szmulowicz, *ibid.* **51**, 1613 (1995); JETP Lett. **60**, 751 (1994); [Pis'ma Zh. Eksp. Teor. Fiz. **60**, 731 (1994)].
[12] M. Tadić and Z. Ikonić, Phys. Rev. B **52**, 8266 (1995).
[13] L. Tsang and S.-L. Chuang, IEEE J. Quantum Electron. **31**, 20 (1995).
[14] B. W. Kim and A. Mejerfeld, J. Appl. Phys. **77**, 4552 (1995); G. Shechter and L. D. Shvartsman, Phys. Rev. B **58**, 3941 (1998).
[15] H. C. Liu, T. Oogarah, E. Dupont, Z. R. Wasilewski, M. Byloos, M. Buchanan, F. Szmulowicz, J. Ehret, and G. J. Brown, Electron. Lett. **38**, 909 (2002).
[16] E. Dupont, M. Gao, Z. Wasilewski, and H. C. Liu, Appl. Phys. Lett. **78**, 2067 (2001).
[17] A. Shen, H. C. Liu, M. Gao, E. Dupont, M. Buchanan, J. Ehret, G. J. Brown, and F. Szmulowicz, Appl. Phys. Lett. **77**, 2400 (2000).
[18] G. Bastard, *Wave Mechanics Applied to Semiconductor Heterostructures* (Halstead, New York, 1988).
[19] A. D. Sánchez and C. R. Proetto, J. Phys. **7**, 2059 (1995); Phys. Rev. B **51**, 17 199 (1995).
[20] F. Szmulowicz, A. Shen, H. C. Liu, G. J. Brown, Z. R. Wasilewski, and M. Buchanan, Phys. Rev. B **61**, 13 798 (2000).
[21] C. Rodriques Bittencourt, A. M. Cohen, and G. E. Marques, Phys. Rev. B **57**, 4525 (1998).
[22] S. Ekbote, M. Cahay, and K. Roenker, Phys. Rev. B **58**, 16 315 (1998); J. Appl. Phys. **85**, 924 (1999).
[23] M. Altarelli, in *Heterojunction and Semiconductor Superlattices*, edited by G. Allen, G. Bastard, N. Baccora, and M. Voos (Springer-Verlag, Berlin, 1986).
[24] D. L. Smith and C. Mailhiot, Phys. Rev. B **33**, 8345 (1986).
[25] H. C. Liu, J. Appl. Phys. **73**, 3062 (1993).

[26] B. A. Foreman, Phys. Rev. B **56**, R12748 (1997).
[27] R. Eppenga, M. F. H. Schuurmans, and S. Colak, Phys. Rev. B **36**, 1554 (1987).
[28] S. M. Hegde, G. J. Brown, F. Szmulowicz, and J. Ehret, Infrared Phys. Technol. **42**, 149 (2001).
[29] P. O. Holtz, Q. X. Zhao, A. C. Ferreira, B. Monemar, M. Sundaram, J. L. Merz, and A. C. Gossard, Phys. Rev. B **48**, 8872 (1993).
[30] C. Ferreira, P. O. Holtz, B. E. Sernelius, I. Buyanova, B. Monemar, O. Mauritz, U. Ekenberg, M. Sundaram, K. Campman, J. L. Merz, and A. C. Gossard, Phys. Rev. B **54**, 16 989 (1996).
[31] C. Ferreira, P. O. Holtz, B. Monemar, M. Sundaram, K. Campman, J. L. Merz, and A. C. Gossard, Phys. Rev. B **54**, 16 994 (1996).